

PLASMONIC EFFECT OF GOLD NANOSPHEROID ON SPONTANEOUS EMISSION

J.-W. Liaw^{1,*}, C.-S. Chen², and J.-H. Chen²

¹Department of Mechanical Engineering, Chang Gung University, 259 Wen-Hwa 1st Rd., Kwei-Shan, Tao-Yuan 333, Taiwan, R.O.C.

²Institute of Applied Mechanics, National Taiwan University, 1, Sec. 4, Roosevelt Rd., Taipei 106, Taiwan, R.O.C.

Abstract—The plasmonic effects of a gold prolate nanospheroid on the spontaneous emission of an adjacent emitter, regarded as an oscillating electric dipole, at the excitation and emission stages are studied respectively by using the multiple multipole method. The numerical results show that when an irradiating light is at the longitudinal surface plasmon resonance frequency of the nanospheroid and with a polarization parallel to the long axis, the strongest excitation rate occurs at the proximity of the long-axis vertex. In addition, if the emitter is at this region, and its orientation is also parallel to the long axis, the apparent quantum yield of the emission is the maximum, compared to the other locations and orientations. Therefore, for this case the overall enhancement factor of a nanospheroid on an emitter's spontaneous emission is the maximum. In contrast, the emitter's emission could be quenched, if it is near the short-axis vertex.

1. INTRODUCTION

Researches over the past decade have shown that the local electric field around a metallic nanoparticle (NP) can be intensified, when the surface plasmon resonance (SPR) mode is excited. Basically SPR is a collective oscillation of free electrons through the whole NP. An important application of SPR is for the enhancement of the spontaneous emission, e.g., the fluorescence of molecule [1–13] or the photoluminescence of quantum dot [14, 15]. Although a metallic nanostructure can indeed induce a strong electric field locally around

Received 14 April 2011, Accepted 13 June 2011, Scheduled 24 June 2011

* Corresponding author: Jiunn-Woei Liaw (markliaw@mail.cgu.edu.tw).

itself, a few of researches showed that sometimes the overall effect of metallic NP on the fluorescence of a nearby molecule could be the quenching [16] rather than the enhancement [8, 9, 11]. The quenching of molecular fluorescence caused by an adjacent metallic NP could be attributed to the absorption and dissipation of energy by metal, particularly when the nonradiative part dominates over the radiative part. The interaction of a spherical NP with a single molecular fluorescence has been studied in several researches [1, 2]. To identify the roles of these metallic nanostructures play on the spontaneous emission, the whole process is divided into two stages [10] for analysis; the first stage is the excitation of an emitter with the aid of the NP, and the second is the following emission of the excited emitter. For the excitation stage, the electric field in the vicinity of a metallic nanostructure is amplified, when the system is stimulated by an irradiating light. Once the emitter is excited, it starts to radiate the fluorescence to the environment as an electric dipole. During the emission stage, the energy transfer between the dipole and the nearby NP also takes place simultaneously. Therefore the multi-roles of the metallic nanostructure play on the spontaneous emission need to be clarified for each stage to assess its overall effect.

Recently, the longitudinal and transverse SPR modes of an elongated NP (e.g., gold nanorod [17–19] or bipyramid [20]) have been widely studied. The former represents the collective motion of free electrons along the long axis, and the latter the short axis. The longitudinal SPR band of an elongated NP is more red-shifted from the SPR band of a spherical NP, as its aspect ratio increases. In contrast, the transverse SPR band is almost equivalent to that of a spherical NP. Moreover, the optical expressions of longitudinal SPR in scattering and absorption are dominant, compared to the transverse one. Because the longitudinal SPR of an elongated NP is tunable, it could be utilized to enhance the fluorescence of a specific molecule on demand. Thus we are motivated to investigate the plasmonic enhancement of a gold nanospheroid on molecular fluorescence.

To analyze the radiation of an emitter near a prolate nanospheroid, the quasi-static model [21] and finite-difference time-domain method [22] were used. Except that, the multiple multipole (MMP) method has been used for the simulation of a plane wave interacting with an ellipsoidal metallic NP [23], and for that of an electric dipole interacting with a spherical NP [24] or dimer [25, 26]. The MMP method was first proposed in 1980 by Hafner [27], which is a semi-analytic method for numerical computations of electromagnetic fields. Basically, the fields are expanded by a series of basis solutions of spherical waves of several poles in MMP method. In investigate the plasmonic effect of a gold

nanospheroid on an emitter's spontaneous emission, MMP method will be adopted in this paper for the analysis of the excitation and emission stages respectively. The effects of the emitter's location and orientation will be particularly considered. Furthermore, the overall effect of a prolate nanospheroid on spontaneous emission will be studied by assessing the enhancement factor.

2. THEORY

The configuration of a prolate nanospheroid, $(x/a)^2 + (y/a)^2 + (z/b)^2 = 1$, and an adjacent emitter (electric dipole) are shown in Fig. 1, where the distance between the dipole and nanospheroid is denoted by d . The wavenumber vector of the incident plane EM wave is denoted by \mathbf{k} , the position vector of the dipole is \mathbf{x}_d , and the unit orientation vector of the dipole is \mathbf{e}_p . There are five typical cases with different locations and orientations of the dipole will be discussed in the following; A: a dipole is under the lower long-axis vertex with a vertical orientation, B: a dipole is under the long-axis vertex but with a horizontal orientation, C: a dipole is beside the short-axis vertex with a horizontal orientation but perpendicular to the surface, D: a dipole is beside the short-axis vertex with a vertical orientation and parallel to the surface, and E: a dipole is beside the short-axis vertex with a horizontal orientation but parallel to the surface. The surrounding medium is air, and the frequent-dependent permittivity of Au in Ref. [28] is used for

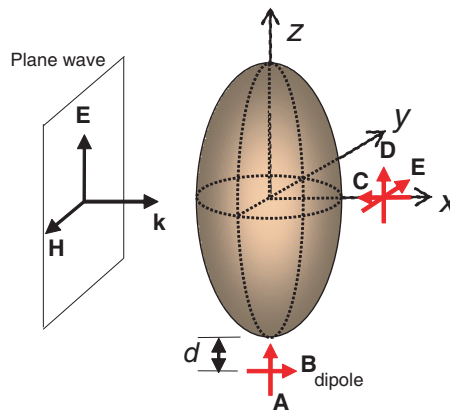


Figure 1. Configuration of Au nanospheroid and a nearby emitter (dipole) with different orientations at different locations irradiated by a plane EM wave.

simulation. A two-stage model of the spontaneous emission is used for analysis; the first stage is the excitation one of the emitter, and the second stage is its subsequent emission. The interactions of a prolate nanospheroid with a plane wave at the excitation stage and with an electric dipole at the emission stage are analyzed individually by using the MMP method for solving Maxwell's equations. The formulation of MMP is referred to our previous work [23].

First, the emitter is assumed unexcited at the initial state. In the excitation stage of this emitter, an incident plane EM wave of wavelength λ_{ex} is used to irradiate a nearby gold nanospheroid, and then a strong near field is induced for exciting the emitter. Using MMP method, the total fields around the nanospheroid are analyzed. The local-field factor at the position of the emitter is further calculated to exhibit the amplification of the electric field caused by the gold nanospheroid for exciting the emitter. The local-field factor K , which is the normalized electric field, is defined as

$$K(\mathbf{x}_d; \lambda_{ex}) = |\mathbf{E}(\mathbf{x}_d; \lambda_{ex})| / |\mathbf{E}^i| \quad (1)$$

where \mathbf{E} is the total electric field at the emitter's position \mathbf{x}_d , and $|\mathbf{E}^i|$ is the amplitude of the electric field of the incident plane wave. Furthermore, the excitation rate $\Psi(\mathbf{x}_d, \mathbf{e}_p; \lambda_{ex})$ upon the emitter is defined by considering the emitter's orientation \mathbf{e}_p ,

$$\Psi(\mathbf{x}_d, \mathbf{e}_p; \lambda_{ex}) = |\mathbf{E}(\mathbf{x}_d; \lambda_{ex}) \cdot \mathbf{e}_p|^2 / |\mathbf{E}^i|^2 \quad (2)$$

Once the emitter (a molecule, or quantum dot) becomes excited, it behaves as an oscillating electric dipole to radiate fluorescence at the emission stage. Since the radiation of the dipole is under the influence of the gold nanospheroid, the interaction of the dipole with the nearby nanospheroid is further studied by employing MMP method also. The dipole's radiative decay rate Γ_r is the power emitted to the far field, and the nonradiative decay rate Γ_{nr} is the dissipating power inside the metal [25, 26]. In this stage, the electric and magnetic fields caused by the electric dipole are denoted by \mathbf{E}_d and \mathbf{H}_d respectively. Both decay rates of an electric dipole in the presence of a nanoparticle at an emission wavelength λ_{em} are expressed in terms of the Poynting vector $\mathbf{E}_d \times \bar{\mathbf{H}}_d$ as,

$$\Gamma_r = \frac{1}{2} \text{Re} \left\{ \int_S \mathbf{E}_d \times \bar{\mathbf{H}}_d \cdot d\mathbf{a} \right\}, \quad (3)$$

$$\Gamma_{nr} = \frac{-1}{2} \text{Re} \left\{ \int_{S_c} \mathbf{E}_d \times \bar{\mathbf{H}}_d \cdot d\mathbf{a} \right\}, \quad (4)$$

where S is any simply closed surface enclosing the dipole and the nanospheroid, S_c is the surface of the nanospheroid, and Re denotes the real part. Here, we assume the surrounding medium is lossless material, e.g., air. In terms of the two decay rates, the apparent quantum yield $\eta(\mathbf{x}_d, \mathbf{e}_p; \lambda_{em})$ is defined as the efficiency of the emission of a dipole in the presence of a nearby nanostructure; $\eta = \Gamma_r / (\Gamma_r + \Gamma_{nr})$ ($0 \leq \eta \leq 1$). Throughout this paper, all quantities of the radiative and nonradiative decay rates are normalized by the radiative one of a free dipole in the absence of a gold NP; i.e., these values are dimensionless. For a free dipole, the apparent quantum yield is unit one in the absence of a metallic NP. From this point, it seems that the apparent quantum yield of a dipole is always reduced in the presence of metallic NP, because the NP induces a nonradiative dissipation at the emission stage. On the other hand, a metallic NP provides a strong excitation rate at the excitation stage. Hence it becomes a trade-off to utilize NP for enhancing the fluorescence.

Finally, to assess the overall plasmonic effect of the metallic nanospheroid on the spontaneous emission of a single emitter, the enhancement factor $\Psi(\mathbf{x}_d, \mathbf{e}_p; \lambda_{ex})\eta(\mathbf{x}_d, \mathbf{e}_p; \lambda_{em})$ is used, where λ_{ex} and λ_{em} are the excitation and emission wavelengths, respectively.

3. NUMERICAL RESULTS AND DISCUSSION

The influences of Au nanospheroid on the excitation and emission stages of an emitter are analyzed individually by MMP method in the following. For MMP method [23, 27], these coefficients of the multiple multi-poles are calculated by matching the boundary conditions (the continuity equations of the electric and magnetic fields) at numerous collocation points distributed on the surface of nanospheroid. Each coefficient in MMP [23] represents the amplitude of a multiple-mode source at a specified location. Using these coefficients, the field distribution of the electric field around the nanospheroid can be further calculated. To identify the SPR characteristic of a gold nanospheroid, the scattering cross section (SCS), absorption cross section (ACS), and extinction cross section (ECS) of a gold nanospheroid ($a = 20$ nm, $b/a = 3$) irradiated by a plane wave ($\mathbf{e}_k = \mathbf{e}_x$) of z -polarization or y -polarization are studied in advance, as shown in Figs. 2(a) and 2(b) respectively, for various excitation wavelengths. All these values are normalized by the projected area of a nanospheroid, $ab\pi$. Fig. 2(a) shows the longitudinal SPR mode with a peak at 620 nm, and Fig. 2(b) the transverse SPR mode with a peak at 520 nm.

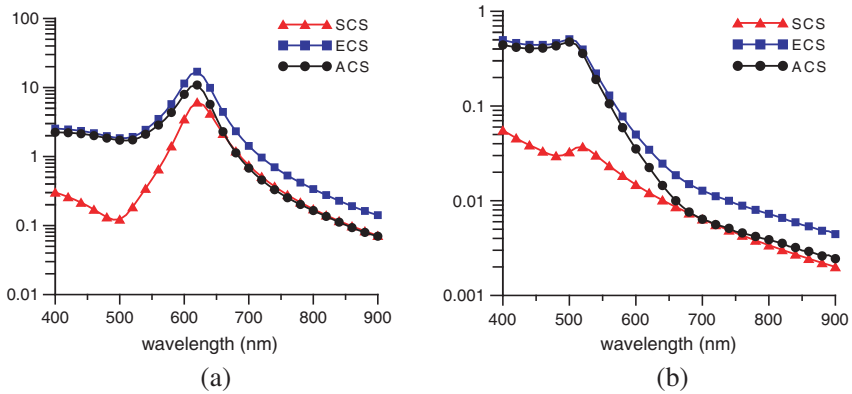


Figure 2. SCS, ACS and ECS of a gold nanospheroid ($a = 20$ nm, $b/a = 3$) irradiated by a plane wave ($\mathbf{e}_k = \mathbf{e}_x$) of (a) z -polarization, and (b) y -polarization at various excitation wavelengths.

3.1. Incident EM Wave Interacting with a Nanospheroid

At the excitation stage, a gold nanospheroid is irradiated by an incident plane EM wave to induce a strong local electric field, which is the pumping source for exciting a nearby emitter. Fig. 3(a) shows the distribution of local-field factor around Au nanospheroid of $a = 20$ nm and $b/a = 3$ irradiated by a z -polarized plane EM wave of $\lambda_{ex} = 650$ nm ($\mathbf{e}_k = \mathbf{e}_x$). For this case, the wavelength is close to the longitudinal SPR (625 nm), as shown in Fig. 1. Hence, the strongest electric fields occur at the long-axis vertices of nanospheroid due to the longitudinal SPR [22,23]. In contrast, the electric field induced by the other excitation wavelength is relatively low, even though at these vertices. Furthermore, Fig. 3(b) shows the excitation rates of Au nanospheroid of $a = 20$ nm with different aspect ratios ($b/a = 1, 1.5, 2, 3$) on a dipole with a long-axis orientation at a location of 10 nm below the long-axis vertex (case A). These curves illustrate that Au nanospheroid with larger aspect ratio can provide a stronger excitation rate in the vicinity of the long-axis vertices. In addition, the peak of the excitation rate is more red-shifted as the aspect ratio increases. For example, for $b/a = 3$ the peak is at 625 nm, which is consistent with the far-field SCS as shown in Fig. 2. Summarily, Au nanospheroid plays a role of a nanolens to focus an incident wave into two small hotspot regions around the long-axis vertices. In contrast, the electric field in the neighborhood of the short-axis vertex is very weak.

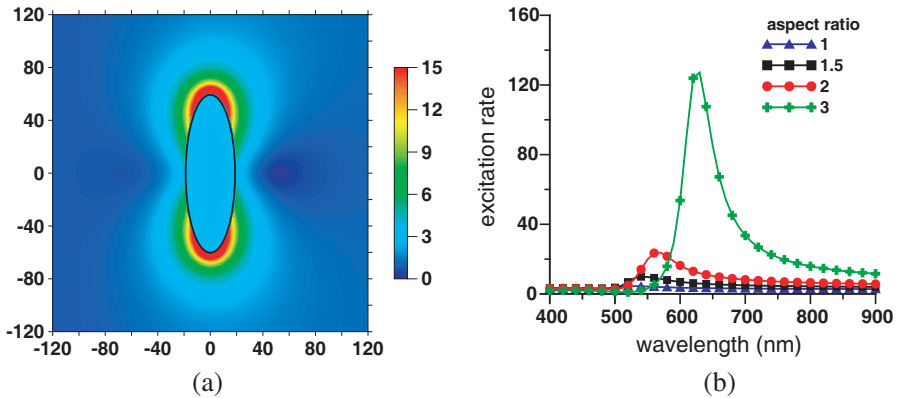


Figure 3. (a) Local-field factor distribution in $x-z$ plane of Fig. 2 at $\lambda_{ex} = 650$ nm. The scale in x and z axes is nanometer. (b) Excitation rates of Au nanospheroid of $a = 20$ nm with different b/a (1, 1.5, 2, 3) on a dipole of case A versus excitation wavelengths, where $d = 10$ nm.

3.2. Dipole Interacting with a Nanospheroid

Once the emitter is excited, its spontaneous emission begins to take place. At the following emission stage, the emitter is modeled as an oscillating dipole. Under the influence of a gold nanospheroid, the radiative and nonradiative decay rates, and the apparent quantum yields of the dipole are affected dramatically. For example, Fig. 4 shows the results of case A for different aspect ratios ($b/a = 1, 1.5, 2,$ or 3), where $a = 20$ nm, and $d = 10$ nm. These radiative decay rates only exhibit the longitudinal mode, as shown in Fig. 4(a). Moreover, the nonradiative decay rates indicate that for $b/a \leq 2$ the longitudinal SPR mode overlaps with the transverse one, while for $b/a = 3$ they separate and the longitudinal one is red-shifted. Hence two peaks for $b/a = 3$ are observed; one is at 520 nm corresponding to the transverse mode, and the other at 625 nm the longitudinal mode. Fig. 4(c) shows that the larger the aspect ratio is, the higher the apparent quantum yield will be, if the emission wavelength is longer than the cut-off wavelength; e.g., for $b/a = 3, \lambda_{em} \geq 600$ nm.

Furthermore, the results of cases A, B, C, D, and E are depicted in Fig. 5 for comparison, where $b/a = 3, d = 10$ nm. The radiative decay rates of cases B, D and E are lower than unit one as shown in Fig. 5(a). For these three cases the radiative part is suppressed by the Au nanospheroid, because the dipole's orientation is parallel to the metal's surface. In contrast, the radiative decay rates of cases A and C are higher than that of a free dipole. This is to say when the dipole's

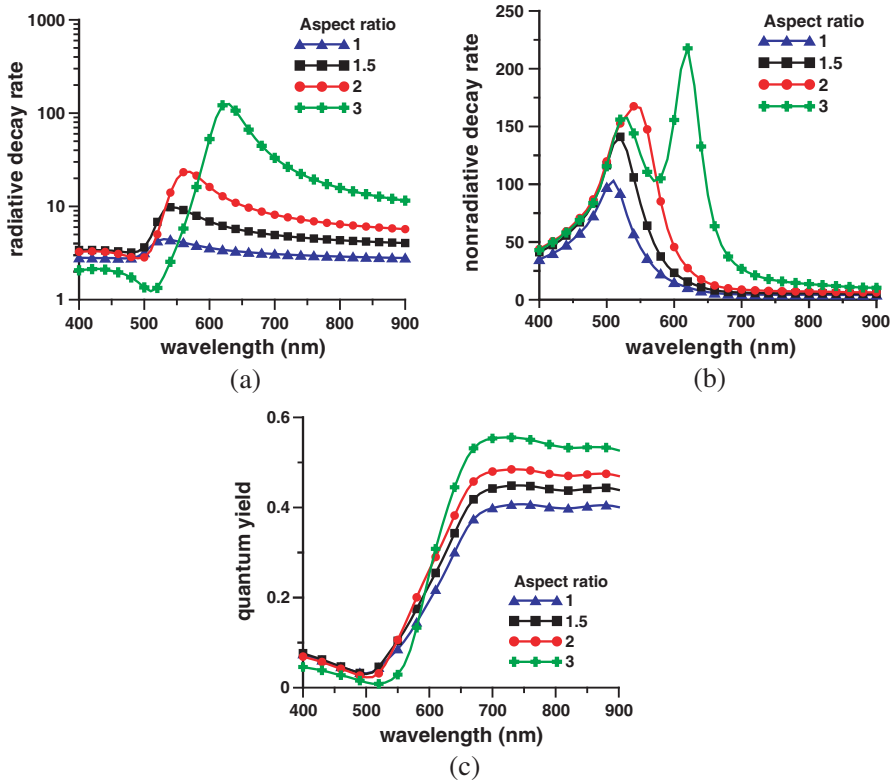


Figure 4. (a) Radiative decay rates. (b) Nonradiative decay rates. (c) Apparent quantum yields versus emission wavelengths for a dipole of case A, where $d = 10$ nm, $a = 20$ nm with different b/a (1, 1.5, 2, 3).

orientation is perpendicular to the metal's surface, the radiative part is enhanced. For the five cases, the common peak of the nonradiative decay rate is at 520 nm of the transverse SPR. However only case A has another peak at 625 nm of the longitudinal SPR, as shown in Fig. 5(b). In addition, the peak of the radiative decay rate of case A is also at 625 nm, as shown in Fig. 5(a). This phenomenon demonstrates that the longitudinal SPR can be easily induced by a dipole near the long-axis vertex and with the long-axis orientation (or at least with this component). For this configuration, an elongated gold nanospheroid behaves as a nanoantenna at the longitudinal SPR mode. However, the energy dissipation rate in metal also increases at this mode. Moreover, the high total decay rate, the sum of the radiative and nonradiative decay rates, at the longitudinal SPR mode implies that the lifetime

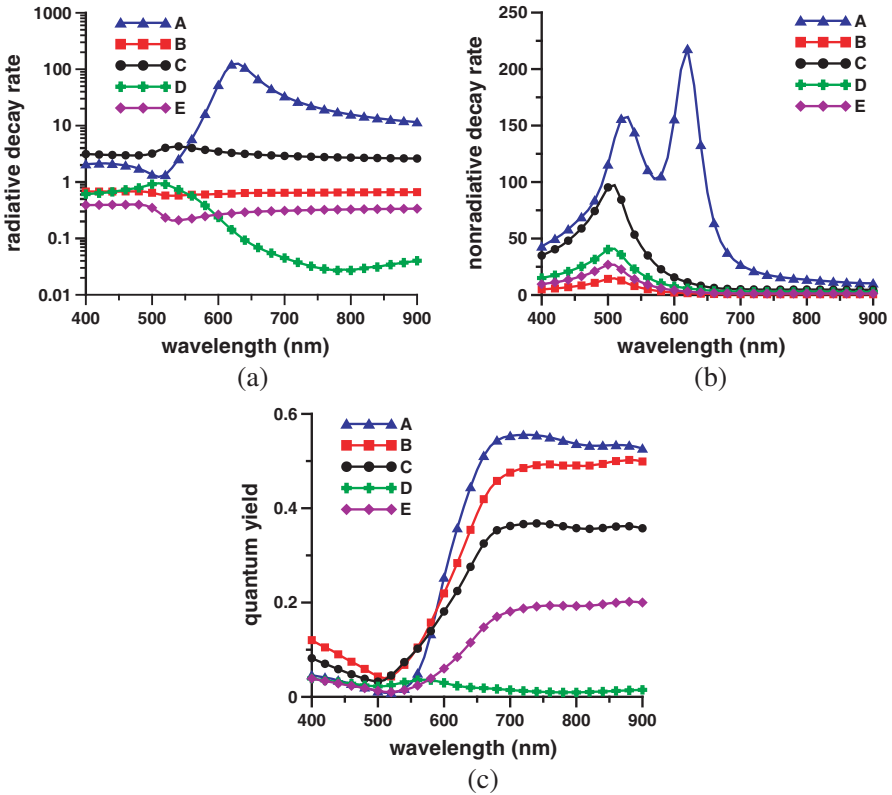


Figure 5. (a) Radiative decay rates. (b) Nonradiative decay rates. (c) Apparent quantum yields versus emission wavelengths for a dipole of different cases (A, B, C, D, E), where $d = 10$ nm, $a = 20$ nm, and $b/a = 3$.

of the spontaneous emission will be reduced dramatically due to the presence of gold nanospheroid for case A. Fig. 5(c) shows that case A has high apparent quantum yield when $\lambda_{em} \geq 600$ nm. This is because that the nonradiative part dominates over the radiative part, if $\lambda_{em} \leq 600$ nm. Therefore, gold nanospheroid is a low-pass filter with a cut-off wavelength for the spontaneous emission. In the other words, most the energy with emission wavelengths short than the cut-off wavelength will be dissipated in the metal.

In contrast, for other cases, the longitudinal SPR mode is difficult to be induced. Furthermore, when the dipole is near the short-axis vertex and with an orientation parallel to the metal surface, the apparent quantum yield is the lowest one, e.g., cases D and E. This

finding implies that an emitter near the short-axis vertex could be quenched rather than enhanced, because the local excitation rate in this area is weak as well as the apparent quantum yield is low.

3.3. Enhancement Factor on Spontaneous Emission

In order to assess the overall plasmonic effect of a gold nanospheroid on the spontaneous emission of a single emitter, the enhancement factor is used. In the following, we assume that there is no Stokes shift between the excitation and the emission wavelengths, (i.e., $\lambda_{em} = \lambda_{ex}$). Therefore the enhancement factor becomes $\Psi(\mathbf{x}_p, \mathbf{e}_p; \lambda)\eta(\mathbf{x}_p, \mathbf{e}_p; \lambda)$. For example, the enhancement factors of gold nanospheroid ($a = 20$ nm) with different aspect ratios ($b/a = 1, 1.5, 2, 3$) on a dipole of case A are depicted in Fig. 6, where $d = 10$ nm. The maximum enhancement factor is 50 at $\lambda = 630$ nm for a gold nanospheroid of $b/a = 3$, which is much larger than that of a spherical NP. Again, this wavelength of 630 nm corresponds to the longitudinal SPR. However when the wavelength is shorter than the cutoff wavelength ($\lambda = 600$ nm), the enhancement factor decreases dramatically for the case of $b/a = 3$. It means that a higher aspect-ratio gold nanospheroid can only enhance the spontaneous emission of emitter with longer-wavelength emission spectra, but is not suitable for those emitters with emission wavelengths shorter than the cut-off wavelength. This

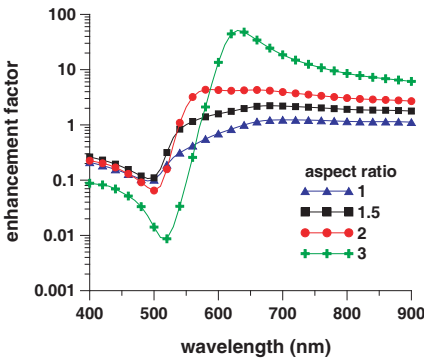


Figure 6. Enhancement factors versus wavelengths for Au nanospheroid of $a = 20$ nm with different $b/a(1, 1.5, 2, 3)$ on the spontaneous emission of an emitter of case A, where $d = 10$ nm.

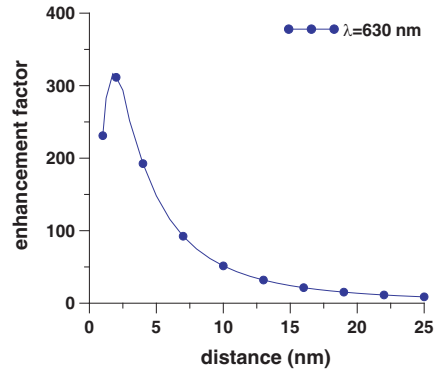


Figure 7. Enhancement factors versus distance d for case A at $\lambda_{ex} = \lambda_{em} = 630$ nm, where $a = 20$ nm and $b/a = 3$.

is because that the longitudinal SPR is red-shifted, as the aspect ratio increases. Moreover, a typical nanospheroid ($a = 20$ nm and $b/a = 3$) for case A is studied to demonstrate the distance effect on the enhancement factor at $\lambda = 630$ nm, as shown in Fig. 7. It indicates that there is an optimal distance to obtain a maximum enhancement factor of 315 at $d = 2.5$ nm. When $d < 2$ nm, the nonradiative decay rate increases abruptly to reduce the apparent quantum yield and the enhancement factor dramatically in turn.

4. CONCLUSIONS

The plasmonic effects of a gold prolate nanospheroid on a vicinal emitter's spontaneous emission are multifunctional. It behaves as a nanolens to focus the irradiating light into hotspots around its long-axis vertices for exciting an emitter within these areas, if the light's polarization and the emitter's orientation are parallel to this axis. On the other hand, it plays another role of a low-pass filter allowing the most energy of the longer wavelength part of the excited emitter radiate to the far field, but dissipating the most of the emission of wavelengths shorter than the cut-off wavelength into Joule's heat. For example, for $b/a = 3$, the cut-off wavelength is 600 nm, which is red-shifted from the interband transition of gold (520 nm). In addition, it is also like a nanoantenna to provide an efficient channel for the energy transfer between a nearby dipole and itself during the dipole's emission, when the dipole is near the long-axis vertex and its orientation is along this axis. Hence, if an emitter is in the proximity of the long-axis vertex of an elongated gold nanospheroid, its spontaneous emission in long-wavelength regime can be enhanced strongly. Moreover, there is an optimal distance between a nanospheroid and a dipole to obtain a maximum enhancement factor. However, if the dipole is located near the long-axis vertex but its orientation is perpendicular to the long axis (case B), the radiative part is suppressed. Hence its apparent quantum yield becomes lower than that of a dipole with an orientation parallel to this axis (case A). In contrast, if the emitter is near the short-axis vertex, the spontaneous emission might be quenched rather than enhanced due to the non-radiative energy transfer from an emitter to a metal NP. In summary, our results illustrate that even though at the longitudinal SPR frequency, the enhancement factor of a gold nanospheroid is sensitive to the location and orientation of the emitter with respect to the NP. In this paper, the emitter is modeled as an ideal dipole without considering its own intrinsic properties. Therefore concerning the plasmonic quenching, the other mechanisms [29] need to be considered further.

ACKNOWLEDGMENT

The research was supported by NSC, Taiwan, R.O.C. (NSC 97-2221-E-182-012-MY2, NSC 99-2221-E-182-030-MY3).

REFERENCES

1. Anger, P., P. Bharadwaj, and L. Novotny, "Enhancement and quenching of single-molecule fluorescence," *Phys. Rev. Lett.*, Vol. 96, 113002, 2006.
2. Kuhn, S., U. Hakanson, L. Rogobete, and V. Sandoghdar, "Enhancement of single-molecule fluorescence using a gold nanoparticle," *Phys. Rev. Lett.*, Vol. 97, 017402, 2006.
3. Colas des Francs, G., A. Bouhelier, E. Finot, J. C. Weeber, A. Dereux, C. Girard, and E. Dujardin, "Fluorescence relaxation in the near-field of a mesoscopic metallic particle: Distance dependence and role of plasmon modes," *Opt. Express*, Vol. 16, 17654, 2008.
4. Ming, T., L. Zhao, Z. Yang, H. Chen, L. Sun, J. Wang, and C. Yan, "Strong polarization dependence of plasmon-enhanced fluorescence on single gold nanorods," *Nano Lett.*, Vol. 9, No. 11, 3896–3903, 2009.
5. Fu, Y., J. Zhang, and J. R. Lakowicz, "Plasmonic enhancement of single-molecule fluorescence near a silver nanoparticle," *J. Fluoresc.*, Vol. 17, 811–816, 2007.
6. Gerber, S., F. Reil, U. Hohenester, T. Schlagenhaufen, J. R. Krenn, and A. Leitner, "Tailoring light emission properties of fluorophores by coupling to resonance-tuned metallic nanostructures," *Phys. Rev. B*, Vol. 75, 073404, 2007.
7. Bharadwaj, P. and L. Novotny, "Spectral dependence of single molecule fluorescence enhancement," *Opt. Express*, Vol. 15, 14266–14274, 2007.
8. Aslan, K., M. Wu, J. R. Lakowicz, and C. D. Geddes, "Metal enhanced fluorescence solution-based sensing platform 2: Fluorescent core-shell Ag@SiO₂ nanoballs," *J. Fluoresc.*, Vol. 17, 127–131, 2007.
9. Tovmachenko, O. G., C. Graf, D. J. Van Den Heuvel, A. Van Blaaderen, and H. C. Gerritsen, "Fluorescence enhancement by metal-core/silica-shell nanoparticles," *Adv. Mater.*, Vol. 18, 91–95, 2006.
10. Liaw, J. W., C. L. Liu, W. M. Tu, C. S. Sun, and M. K. Kuo, "Average enhancement factor of molecules-doped

- coreshell (Ag@SiO₂) on fluorescence,” *Opt. Express*, Vol. 18, No. 12, 12788–12797, 2010.
11. Tam, F., G. P. Goodrich, B. R. Johnson, and N. J. Halas, “Plasmonic enhancement of molecular fluorescence,” *Nano Lett.*, Vol. 7, 496–501, 2007.
 12. Ringler, M., A. Schwemer, M. Wunderlich, A. Nichtl, K. Kurzinger, T. A. Klar, and J. Feldmann, “Shaping emission spectra of fluorescent molecules with single plasmonic nanoresonators,” *Phys. Rev. Lett.*, Vol. 100, 203002, 2008.
 13. Chowdhury, M. H., S. K. Gray, J. Pond, C. D. Geddes, K. Aslan, and J. R. Lakowicz, “Computational study of fluorescence scattering by silver nanoparticles,” *J. Opt. Soc. Am. B*, Vol. 24, 2259–2267, 2007.
 14. Farahani, J. N., D. W. Pohl, H.-J. Eisler, and B. Hecht, “Single quantum dot coupled to a scanning antenna: A tunable superemitter,” *Phys. Rev. Lett.*, Vol. 95, 017402, 2005.
 15. Mertens, H., J. S. Biteen, H. A. Atwater, and A. Polman, “Polarization-selective plasmon-enhanced silicon quantum-dot luminescence,” *Nano Lett.*, Vol. 6, 2622–2625, 2006.
 16. Dulkeith, E., A. C. Morteani, T. Niedereichholz, T. A. Klar, J. Feldmann, S. A. Levi, F. C. J. M. Van Veggel, D. N. Reinhoudt, M. Moller, and D. I. Gittins, “Fluorescence quenching of dye molecules near gold nanoparticles: Radiative and nonradiative effects,” *Phys. Rev. Lett.*, Vol. 89, 203002, 2002.
 17. Eustis, S. and M. A. El-Sayed, “Determination of the aspect ratio statistical distribution of gold nanorods in solution from a theoretical fit of the observed inhomogeneously broadened longitudinal plasmon resonance absorption spectrum,” *J. Appl. Phys.*, Vol. 100, 044324, 2006.
 18. Ni, W., X. Kou, Z. Yang, and J. Wang, “Tailoring longitudinal surface plasmon wavelengths, scattering and absorption cross sections of gold nanorods,” *ACS Nano*, Vol. 2, 677–686, 2008.
 19. Chang, W.-S., J. W. Ha, L. S. Slaughter, and S. Link, “Plasmonic nanorod absorbers as orientation sensors,” *Proc. Natl. Acad. Sci. USA*, Vol. 107, 2781–2786, 2010.
 20. Kou, X., W. Ni, C.-K. Tsung, K. Chan, H.-Q. Lin, G. D. Stucky, and J. Wang, “Growth of gold bipyramids with improved yield and their curvature-directed oxidation,” *Small*, Vol. 3, No. 12, 2103–2113, 2007.
 21. Klimov, V. V., M. Ducloy, and V. S. Letokhov, “Spontaneous emission of an atom placed near a prolate nanospheroid,” *Eur.*

- Phys. J. D*, Vol. 20, 133–148, 2002.
22. Mohammadi, A., V. Sandoghdar, and M. Agio, “Gold nanorods and nanospheroids for enhancing spontaneous emission,” *New J. Phys.*, Vol. 10, 105015, 2008.
 23. Liaw, J. W., M. K. Kuo, and C. N. Liao, “Plasmon resonance of spherical and ellipsoidal nanoparticles,” *Journal of Electromagnetic Waves and Applications*, Vol. 19, No. 13, 1787–1794, 2005.
 24. Hartling, T., P. Reichenbach, and L. M. Eng, “Near-field coupling of a single fluorescent molecule and a spherical gold nanoparticle,” *Opt. Express*, Vol. 5, 12806–12817, 2007.
 25. Liaw, J. W., J. H. Chen, C. S. Chen, and M. K. Kuo, “Purcell effect of nanoshell dimer on single molecule’s fluorescence,” *Opt. Express*, Vol. 17, No. 16, 13532–13540, 2009.
 26. Liaw, J. W., C. S. Chen, and J. H. Chen, “Enhancement or quenching effect of metallic nanodimer on spontaneous emission,” *J. Quant. Spectrosc. Radiat. Transfer*, Vol. 111, 454–465, 2010.
 27. Hafner, C., *The Generalized Multipole Technique for Computational Electromagnetics*, Artech. House, Boston, 1991.
 28. Johnson, P. B. and R. W. Christy, “Optical constants of the noble metals,” *Phys. Rev. B*, Vol. 6, 4370–4379, 1972.
 29. Lakowicz, J. R., “Radiative decay engineering 5: Metal-enhanced fluorescence and plasmon emission,” *Anal. Biochem.*, Vol. 337, 171–194, 2005.